Sensitive and predictable separation of microfluidic droplets by size using in-line passive filter

, W. Lloyd Ung, John A. Heyman, and David A. Weitz

Citation: Biomicrofluidics **11**, 014114 (2017); doi: 10.1063/1.4976723
View online: http://dx.doi.org/10.1063/1.4976723
View Table of Contents: http://aip.scitation.org/toc/bmf/11/1
Published by the American Institute of Physics

Sensitive and predictable separation of microfluidic droplets by size using in-line passive filter

Ruihua Ding (丁睿骅),[1] W. Lloyd Ung,[2] John A. Heyman,[2,3] and David A. Weitz[2]
[1]*Department of Chemistry and Chemical Biology, Harvard University, Cambridge, Massachusetts 02138, USA*
[2]*John A. Paulson School of Engineering and Applied Sciences, Harvard University, Cambridge, Massachusetts 02138, USA*
[3]*SphereBio, Inc., Somerville, Massachusetts 02143, USA*

(Received 22 December 2016; accepted 4 February 2017; published online 21 February 2017)

Active manipulation of droplets is crucial in droplet microfluidics. However, droplet polydispersity decreases the accuracy of active manipulation. We develop a microfluidic "droplet filter" that accurately separates droplets by size. The droplet filter has a sharp size cutoff and is capable of distinguishing droplets differing in volume by 20%. A simple model explains the behavior of the droplets as they pass through the filter. We show application of the filter in improving dielectric sorting efficiency. *Published by AIP Publishing*. [http://dx.doi.org/10.1063/1.4976723]

INTRODUCTION

Droplet microfluidics has shown promise in various fields including directed evolution,[1,2] drug screening,[3,4] and droplet-based nucleic acid analysis.[5,6] Compartmentalization of reactions in small droplets using the microfluidic method increases the sensitivity of assays and reduces the cost.[2,7] An essential component of droplet microfluidics is the active manipulation of droplets such as droplet merging[5,8] and picoinjection,[9] which enable multistep reactions in droplets. In addition, manipulation of droplets via sorting[7,10,11] allows enrichment of desired droplets.

Droplet monodispersity is required for all these active manipulations as devices are designed for droplets of specific size. However, abnormal sized droplets, which are difficult to completely avoid,[7,11] can reduce the efficiency of active manipulations. This is especially problematic in droplet sorting, which is critical for functional screens[7,12] and directed evolution studies.[2] During droplet sorting using an electric field, coalesced droplets, which are slugs, will split at the sorting junction. Broken droplets entering the sort channel become false positives and reduce sorting accuracy. This is detrimental, especially when the desired population is only a small fraction of the total population. Thus, this problem limits the application of droplet microfluidics.

Removal of abnormal-sized droplets on-chip can greatly increase the accuracy of active manipulations; however, this is difficult using current methods. Hydrodynamic methods such as shear-induced migration[13,14] and hydrodynamic separation in Ψ-shaped forked channel[15] can distinguish droplets that differ by a factor of ∼1000 in volume, which is inadequate for accurate sorting. The use of hydrodynamic on-rail filters can achieve sensitive separation by size[16] but this requires fabrication of complicated multi-layered devices. Deterministic lateral displacement (DLD)[17] can separate droplets having a two-fold volume difference;[18,19] however, DLD devices are typically space-consuming, especially when the droplet-size is large. Thus, these methods are unable to sensitively size-separate droplets on a device with limited space and new techniques are required to eliminate the common problem of abnormal sized drops.

Here, we present a new microfluidic design to continuously and precisely separate droplets based on size. In contrast to DLD, which is based on laminar flow and elastic collision, the "droplet filter" is based on the change of Laplace pressure as a droplet is squeezed through a

narrow channel. This simple device successfully separates droplets that are only 20% different in volume. To demonstrate its application in conjunction with other droplet manipulations, we apply this droplet filter upstream of an active sorter. We show that the filter reliably prevents abnormally large droplets from entering the sorting junction and hence improves sorting efficiency.

RESULTS

Droplet filter separates droplets with a precise size cutoff

The droplet filter consists of several rows of equally spaced posts within a polydimethylsiloxane (PDMS) microfluidic device. Droplets enter the filter junction from one side as shown in the schematic of the filter in Fig. 1(a). Hydrodynamic flow is induced in both positive x and positive y directions. Smaller droplets (shown in blue) can move freely through the gaps in the filter or squeeze through the gaps after some deformation. In contrast, large droplets (shown in red) will not pass through the filter, as the flow-induced forces cannot overcome the surface tension during the shape change. These droplets are "rejected" and only move along the y direction to exit the filter region.

To test the sensitivity of this principle, we designed a device to observe droplet behavior at a single-row filter (Figs. 1(b) and S1 (supplementary material)). Highly monodisperse water-in-oil droplets generated by a flow-focusing dropmaker[20] (not shown) enter through the droplet channel. We inject extra oil from the spacing oil inlet to further separate droplets and minimize pressure fluctuations in the filter junction. The spacing oil also forces the droplets to the filter side of the channel, ensuring that all droplets enter the filter junction from the same location. At the filter junction, the main oil streamline crosses the filter as this path to the outlet has lower resistance. Rejected droplets reach the outlet by moving though the narrower channel.

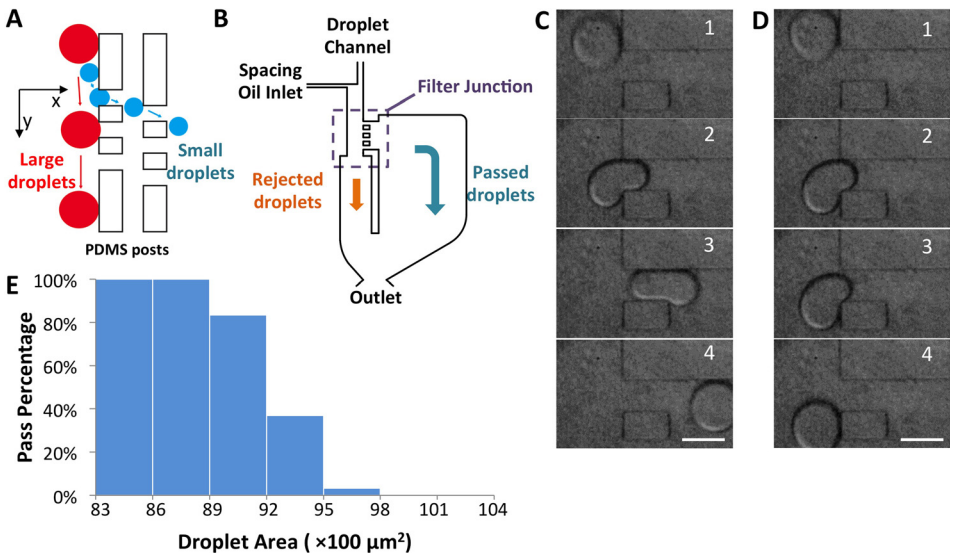

FIG. 1. Filter separates droplets with a sharp size cutoff. (a) Separation principle. Droplets approach the PDMS posts from top-left. Flow-induced force is present in both positive y and positive x directions. Small droplets (blue) move between gaps of the filter down the pressure gradient. Large droplets (red) cannot squeeze though the gaps due to Laplace pressure and move only in the y direction. (b) Design of the single layer filter device. Droplets enter from the droplet channel and are further separated by the spacing oil before entering the filter junction (purple dashed square). Rejected droplets enter the narrower downstream channel while the passed droplets enter the wider downstream channel. All droplets flow to the same outlet. For drawing clarity, the spacing oil inlet has been widened and posts supporting the channels have been omitted. (c) Serial images of a single droplet passing through a gap of a filter. (d) Serial images of a single droplet being rejected by the same filter gap. (e) Percentage of droplets of a given projected area that passed through a filter channel with 67.5 μm gaps. Scale bars: 100 μm.

We generate droplets with different sizes and use a high-speed camera to record their behavior in the droplet filter region. Droplets dramatically slow down and deform into a "bean" shape as they contact the first filter channel (Figs. 1(c2) and 1(d2)). Smaller droplets further deform and squeeze through the filter (Fig. 1(c1–4); SI Movie 1 (supplementary material)). In contrast, larger droplets return to their circular shape as they move away from the filter channel (Fig. 1(d1–4); SI Movie 2 (supplementary material)). Using a device with a filter having a 67.5 μm gap, we analyze over 500 droplets and determine droplet size by measuring the projected area they span inside the device. This area can be directly obtained by analyzing the images of the droplets in the device. Because droplets are squeezed into a pancake shape in the device, the droplet volume is the projected area multiplied by the channel height. All droplets below 8900 μm^2 pass through the filter and all droplets above 9800 μm^2 are rejected (Fig. 1(e)). This shows that our design can distinguish droplets that are 20% different in volume. We define the size at which 50% of the droplets pass as the "critical droplet size" of the particular filter. The filter rejects all drops 10% larger than the critical drop size.

Filter behavior can be explained by a simple model

To elucidate the relationship between the filter design and the corresponding critical droplet size, we analyze the net force on droplets as they enter the filter junction. As observed, the droplets are nearly static at the "bean-shaped" state as in Fig. 1(d2) before re-accelerating to enter or leave the filter channel. This indicates that the "bean-shaped" state is the critical state at which the net force on the droplet determines its direction. If the net force on the droplet is in the positive x direction, the droplet can squeeze through the filter channel; if not, the droplet will be rejected by the filter and move in the positive y direction.

We model the bean shape with three arcs (Fig. 2(a)): (1) a half-circle with radius R_1 half of the gap size L between posts at the entrance of the filter channel; (2) a quarter-circle with radius R_2 outside the channel; and (3) a half-circle with radius $R_3 = 0.5 \cdot R_2$ downstream of R_2. The projected droplet area A can be expressed as

$$A = \frac{\pi {R_1}^2}{2} + \frac{\pi {R_2}^2}{4} + \frac{\pi {R_3}^2}{2} = \frac{3\pi {R_2}^2}{8} + \frac{\pi L^2}{8}. \tag{1}$$

Each of these three arcs generates Laplace pressure on the droplet. The two principal radii of the surface are the radius of the arc and half of the channel height h. The surface tension σ is measured as 7.6 mN/m using the pendant drop method. Thus, the arc with radius R_1 generates a net pressure in the negative x direction with a net force

$$F_{1x} = P_{1x} \times L \times h = \sigma \left(\frac{1}{R_1} + \frac{2}{h} \right) \times L \times h. \tag{2}$$

The pressure from the quarter-circle can be viewed as two equal sub-pressures in the positive x and positive y directions. For the y direction, the force on the droplet can be expressed as

$$F_{2y} = P_{2y} \times R_2 \times h = \sigma \left(\frac{1}{R_2} + \frac{2}{h} \right) \times R_2 \times h. \tag{3}$$

For the x direction, on the part below the dashed line of Fig. 2(b), the normal force from the PDMS post balances all other forces in the x direction. Therefore, it is only necessary to consider the net x direction force above the dashed line. Thus, the force from this pressure in the x direction is

$$F_{2x} = P_{2x} \times L \times h = \sigma \left(\frac{1}{R_2} + \frac{2}{h} \right) \times L \times h. \tag{4}$$

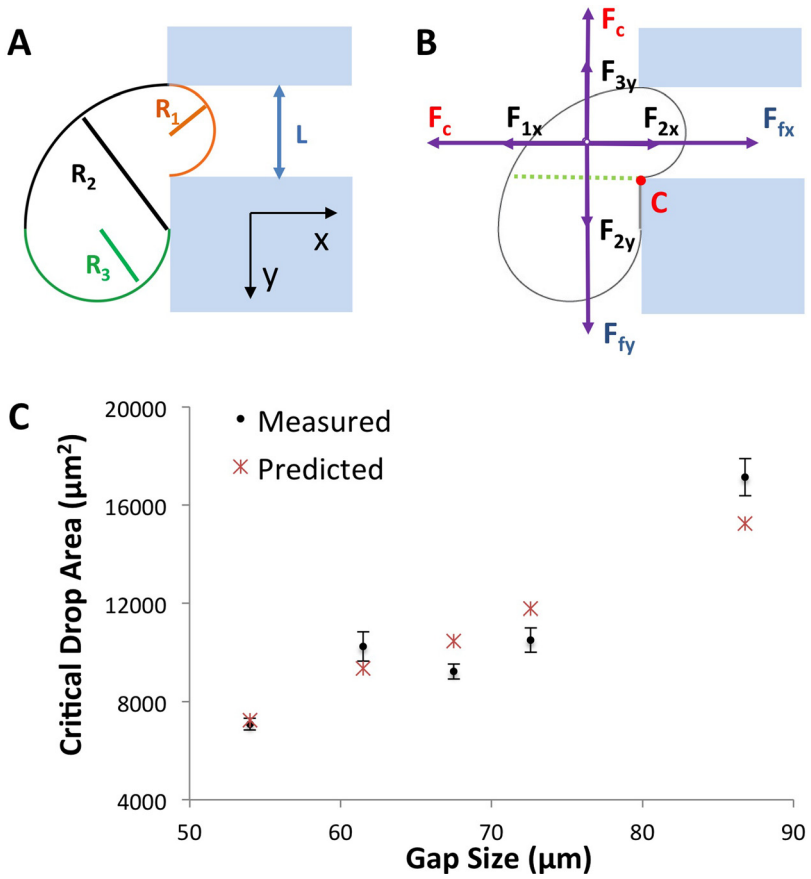

FIG. 2. A simple model predicting filter performance. (a) Model of the droplet shape at the critical "bean" state. (b) Forces acting on the droplet at the critical state. (c) The measured and model-predicted critical droplet size (in projected area) for devices with filters of different gaps. For each point, droplets within the error bars have a 20%–80% likelihood of passing through the filter.

Similarly, the half-circle with radius R_3 gives Laplace pressure in the negative y direction. The force it exerts is

$$F_{3y} = P_{3y} \times R_2 \times h = \sigma\left(\frac{1}{R_3} + \frac{2}{h}\right) \times R_2 \times h. \tag{5}$$

In addition, a fourth surface tension is generated by the curvature at point C (Fig. 2(b)) with the same force, F_c, in the negative x and negative y directions. To calculate F_c, we examine the force balance in the y direction. As a droplet passes through the filter, it is static in the y direction, indicating force balance in this direction. Assuming negligible internal flow due to the small size of the droplet, F_c balances the flow-induced force F_{fy} and the surface tensions in the y direction

$$F_c = F_{fy} + F_{2y} - F_{3y}. \tag{6}$$

Whether the droplet can pass the filter is determined by the x direction net force

$$\begin{aligned} F_{xnet} &= F_{fx} + F_{2x} - F_{1x} - F_c \\ &= F_{fx} - F_{fy} + \left(\frac{L}{R_2} - 1\right)\sigma \times h, \end{aligned} \tag{7}$$

where F_{fx} is the flow-induced force in the x direction.

If F_{xnet} is positive, the droplet will enter further into the channel. This will decrease R_2 and further increase F_{xnet}, eventually letting the droplet pass through the filter. In contrast, if F_{xnet} is negative, the droplet will move away from the filter and thus be rejected.

To determine if this model agrees with the experimental data, we measure the critical droplet area of 5 devices with L between 50 and 90 μm. We calculate the flow-induced forces for all 5 devices and derive the predicted critical droplet area from the measured device dimensions. The predicted and measured critical droplet area for each device is plotted in Fig. 2(d). In all cases, the predicted value is within 15% of the measured value.

Droplet filter removes false positives before active sorting

To demonstrate the practical application of the droplet filter, we use it to remove large droplets upstream of a dielectric sorting junction.[10] We design a sorter that consists of three parts: droplet filtering region, dielectric sorting region, and observation trap (Fig. 3; SI Fig. 2 (supplementary material)). The droplet filtering region is furthest upstream. Droplets are injected from inlet *a*. The spacing oil from inlet *b* separates droplets and pushes them towards the filter. We use multiple rows of PDMS posts to ensure the speed and accuracy of passive filtering. The large droplets rejected by the filter exit the device from outlet *c*. Only the droplets that pass through the filter move downstream to the dielectric sorting region. Because off-chip handling may induce coalescence, we aim to access the sorted droplets on-chip. Thus, we design an observation trap downstream of the sorting channel, using a strategy similar to that previously reported.[21] The trap consists of arrays of PDMS posts with 10 μm spacing. The arrays enclose a square area in the path of the flow. Sorted droplets are trapped in this square area while excess oil escapes through the gaps between the posts. Two outlets are designed for the trap. During initial flow stabilization, the downstream outlet *i* is plugged and debris exit the device from outlet *h* instead of entering the trap. During sorting, the outlet *h* can be plugged and the sorted droplets can be directed into the trap as oil exits through the downstream outlet *i*.

To test if the filter prevents large droplets from entering the sorting junction, we use a highly polydisperse population of droplets created by intentionally coalescing monodisperse rhodamine6G (Sigma R4127)-filled droplets (Fig. 4(a)). We inject these droplets into the sorting device and detect their fluorescence as they pass though the fluorescence detection region (Fig. 3(e)). Droplets are squeezed into an elongated shape in the channel; thus, their passing time through the fluorescence detection region is directly proportional to their size. In these

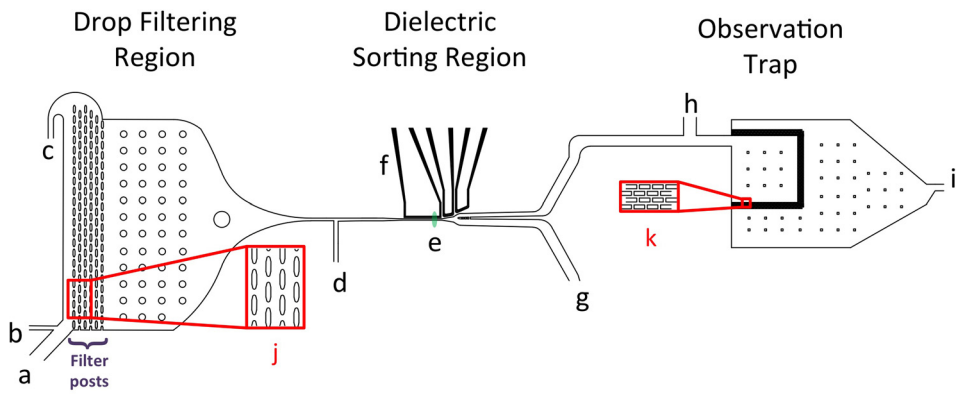

FIG. 3. Sorting device design. Droplets are injected from inlet "a." Oil from inlet "b" serves to space droplets and press them towards the filter. Large droplets get rejected and exit from outlet "c." The droplets that pass through the filter move toward the sorting junction, where they are further spaced by oil entering from inlet "d." Within the sorting junction, the droplets pass through a laser slit at "e" and their fluorescence is detected. A temporary AC electrical field generated by the triggered activation of electrodes "f" sorts desired droplets. Unsorted droplets exit from outlet "g." Sorted droplets are retained in the observation trap. Outlet "h" is used in initial flow stabilization and is plugged during sorting. Outlet "i" allows oil to leave the device while droplets are retained in the trap. "j" shows the magnified filter. "k" shows the magnified trap posts. For simplicity some flow resistors are omitted.

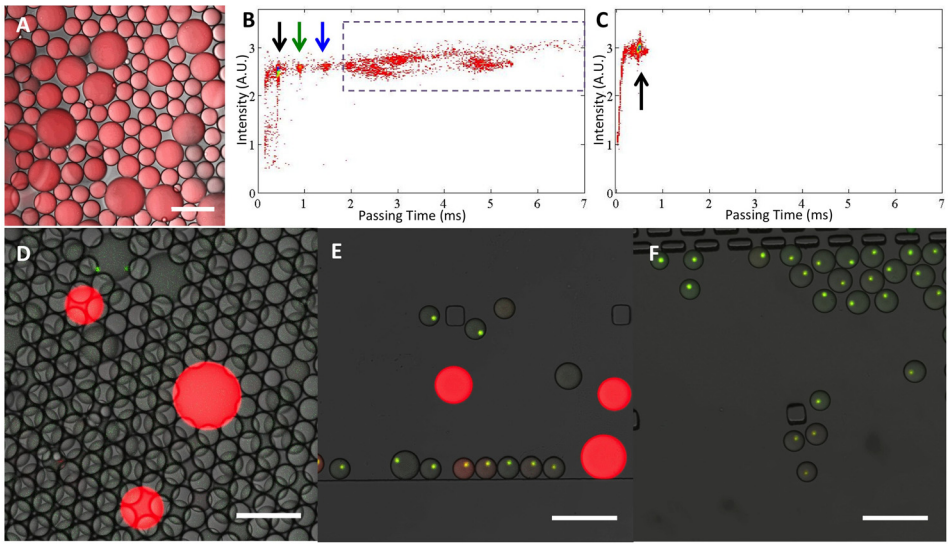

FIG. 4. Filter increases the effectiveness of sorting. (a)–(c): Passive filter efficiently removes merged droplets. Intentionally merged Rhodamine droplets (a) are injected into sorting devices. The detected passing time (proportional to droplet size) and fluorescent intensity of droplets detected at sorting junction without (b) or with (c) a filter upstream of the sorter. Each experiment has more than 8000 events detected. Black arrows show the unmerged droplets. Green and blue arrows show doublet and triplet merged droplets. Dashed purple rectangle denotes larger merged droplets. (d)–(f): Passive filter increases the purity of sorted droplets. The input consists of monodisperse droplets containing fluorescent beads and larger, polydisperse droplets with red fluorescent dye (d). The droplets are sorted based on the presence of bright green fluorescent beads. Droplets sorted without (e) or with (f) filter upstream of the sorter are imaged in the observation trap. Scale bars: 100 μm.

experiments, the unmerged droplets require 0.5 ms to pass the detection region. When we use a sorter lacking a droplet filter, populations of doublet and triplet (Fig. 4(b), green and blue arrows, respectively) merged droplets can clearly be identified. Larger merged droplets, split by the spacing oil and not in distinct groups, are also clearly present (Fig. 4(b), purple dashed box). In stark contrast, when we use a sorter with the droplet filter, no merged droplets are detected (Fig. 4(c)). This indicates that the droplet filter successfully prevents abnormally large droplets from entering the active sorting junction.

We next test whether removal of large droplets by the droplet filter removes false positives during sorting. Monodisperse droplets are made with weak green fluorescence and ~5% of them contain a highly fluorescent bead. Large droplets with red fluorescence but no green fluorescence are spiked in to mimic abnormally large droplets (Fig. 4(d)). We sort droplets based on the strong green fluorescence from the beads. As expected, a device without a droplet filter sorts positive droplets. However, large red droplets are also present in the trap, indicating that large droplets enter the sorting channel and lead to false positives (Fig. 4(e)). With the droplet filter upstream, however, no red droplets are found inside the trap (Fig. 4(f)). Thus, the droplet filter effectively removes false positives during active sorting by removing abnormally large droplets.

CONCLUSION

We demonstrate a microfluidic droplet filter that efficiently separates droplets based on size. The filter is much more accurate than previously reported methods and can distinguish droplets having only a 20% difference in volume. We develop a simple physical model that explains the droplet behavior at the filter junction and predicts the critical droplet size, the size above which the droplet gets rejected. The droplet filter can be used in conjunction with other manipulation methods. We show that placing the filter upstream of a dielectric sorter removes larger droplets and greatly improves the sorting accuracy.

MATERIALS AND METHODS

Device fabrication

Devices are fabricated using standard soft lithography. Masks are printed onto a transparency (CAD/Art Services, Inc., Bandon, OR). SU8-2025 (Microchem, Newton, MA, USA) is spincoated onto a clean silicon wafer (3-in. diameter, Type-P, 1S polished; University Wafer, S3P01SP). UV exposure is used to crosslink the pattern and uncrosslinked photoresist is removed using propylene glycol monomethyl ether acetate (PGMEA; Sigma-Aldrich 537543). For all devices, the feature height is $\sim 25\,\mu$m. The wafer is then treated with 0.2% 1H,1H,2H,2H-Perfluorododecyltrichlorosilane (Sigma-Aldrich 448931) for 10–15 min. PDMS (Sylgard 184 Silicone Elastomer, Dow Corning, Midland, MI) is mixed with curing agent 10:1 by weight. The mixture is degassed and poured onto the SU-8 mold. The device is then cured at 65 °C for more than 5 h before the PDMS is carefully peeled off from the mold. Holes connecting to the channels are formed using biopsy punches (2 mm diameter Harris Uni-Core, Ted Pella, Inc., Redding, CA). The device is then bonded to a clean glass slide after plasma activating both surfaces. Electrodes for sorting are fabricated on chip using a low melting temperature solder (The Indium Corporation of America, wirebn-53307). Aquapel (PPG Industries, Pittsburgh, PA) is then flushed through channels to ensure that the inner surfaces are hydrophobic.

Experimental set up

For all experiments, HFE-7500 (3M, USA) is used as a continuous phase and the dispersed phase is aqueous (phosphate buffered saline). We used 2% (w/v) fluorinated surfactant (008-FluoroSurfactant, Ran Biotechnologies, USA) in dropmaking oil and 0.2% in spacing oil. Syringe pumps (PHD 2000/2200, Harvard Apparatus, Holliston, MA) are used to control flow rates. For sensitivity tests, the typical flow rate is more than 300 μl/h for spacing oil, more than 100 μl/h for dropmaking oil, and about 10 μl/h for the aqueous phase. The droplet size can be varied by changing aqueous speed; in these experiments, the total speed is changed by less than 2%. For all devices, $F_{fx} - F_{fy}$ is between 30 nN and 60 nN. The device is imaged using a fast camera (Phantom V5.1, Vision Research Inc.) connected to the eyepiece of a microscope though an adaptor.

For sorting experiments, we used Sphero Rainbow calibration beads (Spherotech RCP-60-5-5). The red and green dyes are CellTracker Deep Red (ThermoScientific C34565) and Alexa 488, respectively. The fluorescence is detected via photomultiplier tubes.[7] Pictures are taken using a confocal microscope (Leica SP-5).

Model building

Device dimensions are measured using a surface profiler (P-16+ KLA- Tencor) and confocal microscope (Leica SP-5). Channel resistances are calculated using the formula $\frac{12\times\mu\times l}{W\cdot h^3\cdot\left(1-0.63\cdot\frac{h}{W}\right)}$, where μ is the viscosity of the liquid, l is the length of the channel, W is the width of the channel and it is larger than h, the channel height. The device is then approximated as an electrical circuit and the flow rates are calculated using the PartSim circuit simulator (www.partsim.com).

SUPPLEMENTARY MATERIAL

See supplementary material for complete design of devices for sensitivity tests and sorting. Movies showing droplets passing or getting rejected by a filter can also be found.

ACKNOWLEDGMENTS

This work was supported by the National Science Foundation (DMR-1310266) and the Harvard Materials Research Science and Engineering Center (DMR-1420570).

Device fabrication and channel height measurements are performed in Harvard University

Center for Nanoscale Systems (CNS), a member of the National Nanotechnology Coordinated Infrastructure Network (NNCI).

[1]B. Kintses, C. Hein, M. F. Mohamed, M. Fischlechner, F. Courtois, C. Leine, and F. Hollfelder, Chem. Biol. **19**, 1001–1009 (2012).
[2]J. J. Agresti, E. Antipov, A. R. Abate, K. Ahn, A. C. Rowat, J. C. Baret, M. Marquez, A. M. Klibanov, A. D. Griffiths, and D. A. Weitz, Proc. Natl. Acad. Sci. U.S.A. **107**, 4004–4009 (2010).
[3]K. Churski, T. S. Kaminski, S. Jakiela, W. Kamysz, W. Baranska-Rybak, D. B. Weibel, and P. Garstecki, Lab Chip **12**, 1629–1637 (2012).
[4]O. J. Miller, A. El Harrak, T. Mangeat, J. C. Baret, L. Frenz, B. El Debs, E. Mayot, M. L. Samuels, E. K. Rooney, P. Dieu, M. Galvan, D. R. Link, and A. D. Griffiths, Proc. Natl. Acad. Sci. U.S.A. **109**, 378–383 (2012).
[5]R. Tewhey, J. B. Warner, M. Nakano, B. Libby, M. Medkova, P. H. David, S. K. Kotsopoulos, M. L. Samuels, J. B. Hutchison, J. W. Larson, E. J. Topol, M. P. Weiner, O. Harismendy, J. Olson, D. R. Link, and K. A. Frazer, Nat. Biotechnol.**27**, 1025–U1094 (2009).
[6]A. Rotem, O. Ram, N. Shoresh, R. A. Sperling, M. Schnall-Levin, H. D. Zhang, A. Basu, B. E. Bernstein, and D. A. Weitz, PLoS One **10**, e0116328 (2015).
[7]L. Mazutis, J. Gilbert, W. L. Ung, D. A. Weitz, A. D. Griffiths, and J. A. Heyman, Nat. Protoc.**8**, 870–891 (2013).
[8]M. Chabert, K. D. Dorfman, and J. L. Viovy, Electrophoresis **26**, 3706–3715 (2005).
[9]A. R. Abate, T. Hung, P. Mary, J. J. Agresti, and D. A. Weitz, Proc. Natl. Acad. Sci. U.S.A. **107**, 19163–19166 (2010).
[10]K. Ahn, C. Kerbage, T. P. Hunt, R. M. Westervelt, D. R. Link, and D. A. Weitz, Appl. Phys. Lett. **88**, 024104 (2006).
[11]J. C. Baret, O. J. Miller, V. Taly, M. Ryckelynck, A. El-Harrak, L. Frenz, C. Rick, M. L. Samuels, J. B. Hutchison, J. J. Agresti, D. R. Link, D. A. Weitz, and A. D. Griffiths, Lab Chip **9**, 1850–1858 (2009).
[12]N. W. Cui, H. D. Zhang, N. Schneider, Y. Tao, H. Asahara, Z. Y. Sun, Y. M. Cai, S. A. Koehler, T. F. A. de Greef, A. Abbaspourrad, D. A. Weitz, and S. R. Chong, Sci. Rep.-Uk **6**, 22575 (2016).
[13]Y. C. Tan and A. P. Lee, Lab Chip **5**, 1178–1183 (2005).
[14]M. Chabert and J. L. Viovy, Proc. Natl. Acad. Sci. U.S.A. **105**, 3191–3196 (2008).
[15]G. D. M. Jeffries, J. S. Kuo, and D. T. Chiu, Angew. Chem. Int. Ed. **46**, 1326–1328 (2007).
[16]D. H. Yoon, S. Numakunai, A. Nakahara, T. Sekiguchi, and S. Shoji, RSC Adv.**4**, 37721–37725 (2014).
[17]L. R. Huang, E. C. Cox, R. H. Austin, and J. C. Sturm, Science **304**, 987–990 (2004).
[18]H. N. Joensson, M. Uhlen, and H. A. Svahn, Lab Chip **11**, 1305–1310 (2011).
[19]T. Bowman, J. Frechette, and G. Drazer, Lab Chip **12**, 2903–2908 (2012).
[20]S. L. Anna, N. Bontoux, and H. A. Stone, Appl. Phys. Lett. **82**, 364–366 (2003).
[21]M. Zagnoni and J. M. Cooper, Lab Chip **10**, 3069–3073 (2010).